J. Fluid Mech. (1988), *vol.* 194, *pp.* 153–173
Printed in Great Britain

On the preferred mode of jet instability

By R. A. PETERSEN AND M. M. SAMET
Department of Aerospace and Mechanical Engineering, University of Arizona, Tucson, AZ 85721, USA

(Received 16 January 1987 and in revised form 24 September 1987)

The preferred mode of instability was investigated in an axisymmetric air jet of moderate Reynolds number. Natural instabilities are shown to scale with local shear-layer thickness and the preferred mode is shown to be a shear-layer instability. The spatial evolution of the preferred mode was examined by exciting the flow acoustically and then mapping the phase-locked velocity fluctuations. Throughout the potential core region the phase-locked profiles are shown to agree with the eigensolutions of the Orr–Sommerfeld stability equations provided the calculations are based on measured, mean velocity profiles. The excitation intensity was varied from low levels, where the flow was merely tagged, to high levels where the mean flow was substantially distorted, and over that range of excitation there was no apparent deterioration in the agreement with stability predictions.

1. Introduction

The concept of a preferred mode of jet instability was introduced by Crow & Champagne (1971) to describe the response of their axisymmetric jet to externally imposed, axisymmetric excitations. The term was used to denote the mode that attained the maximum growth under nonlinear saturation. Their measurements were taken at a fixed location on the jet centreline 4 diameters downstream from the jet exit plane. The frequency of the preferred mode was observed to scale with jet velocity U_j and diameter D such that $f = 0.3U_j/D$, and they conjectured that the mode was a global instability of the entire jet column.

Since that time there has been controversy concerning the physical mechanism of the preferred mode. Some investigators (e.g. Kibens 1981; Hussain & Zaman 1981) distinguish two different types of jet instability: a shear-layer mode and the preferred mode. According to that point of view, the shear-layer mode is an inflexional instability of the initial shear layer where the frequency scales with the shear-layer thickness, whereas the preferred mode is a global instability of the entire jet column where the frequency scales with jet diameter. On the other hand several theoretical models have been developed based solely on shear-layer instabilities. For example, Crighton & Gaster (1976) considered the Rayleigh instability of a hyperbolic tangent velocity profile that grew in the streamwise direction. By using a multiple scales analysis to predict the spatial evolution of the perturbation amplitude, the wave with maximum total amplification at $x/D = 4$ was calculated to have a Strouhal number near 0.38. This value is within the range of Strouhal numbers reported by various investigators for the preferred mode (Gutmark & Ho 1983). Also, energy integral techniques have been reasonably successful in predicting the nonlinear evolution of pressure amplitudes in acoustically excited jets (Chan 1977; Tam & Morris 1985). The integral formulation requires a shape assumption to

account for transverse distributions of turbulence quantities. These shape assumptions are based on eigenfunctions of the Rayleigh equation which describes a shear-layer instability.

The aim of the present study is to demonstrate that there is no distinction between shear-layer modes and the preferred mode. First it will be shown that naturally occurring instabilities in an unforced jet scale with local momentum thickness at all streamwise locations within the potential-core region. Then the Crow & Champagne instability will be excited acoustically and its spatial evolution along the jet core will be mapped. Based on phase-locked measurements of velocity fluctuations compared to Orr–Sommerfeld stability calculations it will be shown that the preferred mode is actually the shear-layer mode that is most amplified by $x/D = 4$. By implication there is no such thing as a single preferred mode. The most amplified shear-layer instability depends on streamwise location and on the streamwise distribution of shear-layer thickness.

This investigation was motivated by recent experiments (reviewed by Wygnanski & Petersen 1987) that have demonstrated that profiles of phase-locked velocity fluctuations can be predicted from linear, spatial stability theory. The experiments have encompassed a wide range of geometries including the plane wake, the plane mixing layer, as well as the axisymmetric jet. The agreement is quite good even when the flow is fully turbulent provided the calculations are based on the measured, mean velocity profile. In the case of an axisymmetric mixing layer the stability eigenvalues scale with local shear-layer thickness; jet diameter enters the calculations as a parameter and as long as the ratio of momentum thickness to jet diameter is small it is not a very sensitive parameter (Michalke 1971; Michalke & Hermann 1982).

2. Experimental facility

The experiments were carried out in the jet facility shown in figure 1. The nozzle was used in the original Crow & Champagne experiment and the contour consisted of two tangent arcs. The exit diameter was 50.8 mm and the area contraction ratio was 36 : 1. The plenum chamber housed two air filters, a honeycomb and three screens to minimize flow disturbances. A pressure-regulated air supply was delivered through a system of driers, reservoirs and filters. The exit velocity could be controlled to an accuracy of $\pm 1\,\%$. The jet emerged with a top-hat velocity profile and the free shear layer was initially laminar. The measurements reported in this study were conducted at an exit velocity of 16 m/s, which corresponds to a Reynolds number of 5.6×10^4 based on nozzle diameter and exit velocity. The free-stream turbulence level at this speed was 0.11 % and was measured on the centreline at the nozzle exit. The entire jet was enclosed in a large cage made from $\frac{1}{6}$ mm mesh screen to minimize the effects of room draughts.

The streamwise component of velocity was measured with a circumferential array of eight hot-wire sensors each 1.25 mm in length made from 5 μm platinum-plated tungsten wire. The probes were spaced at equal circumferential angles on a radial traverse mechanism and the probe holders were inclined at an angle of 60° with respect to the jet axis. At this orientation, the interference of the probes with the flow was minimized. The traverse mechanism was driven under computer control by a stepper motor and all eight probes moved simultaneously in the radial direction. The individual probes were aligned radially at the half-velocity point and an optical cathetometer was used to position the wires in the streamwise direction.

Hot-wire data were acquired and analysed digitally. The hot-wire signals were

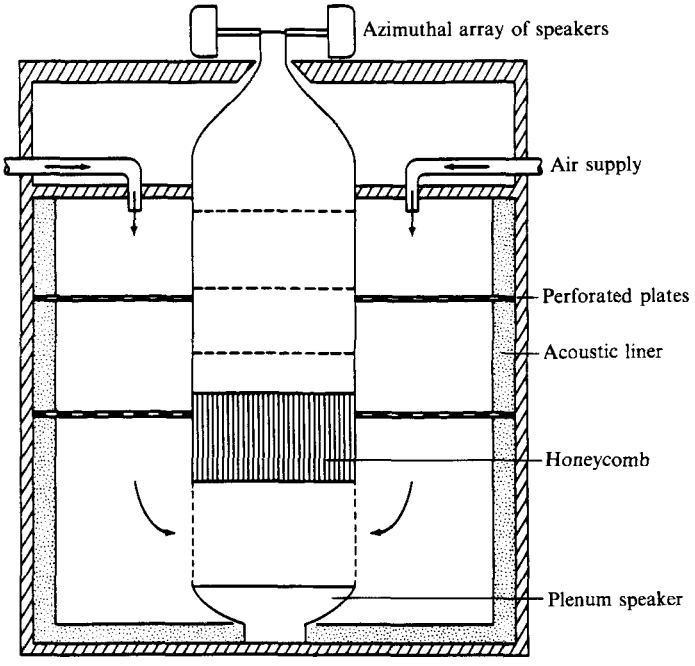

FIGURE 1. Air-jet facility.

conditioned by passing them through a network of buck-and-gain amplifiers followed by a network of low-pass filters with cutoff frequencies of 10 kHz. They were then digitized to 16-bit resolution. The hot-wire signals were linearized digitally using a fourth-order calibration polynomial.

Controlled excitation of the flow was accomplished acoustically using an array of eight speakers arranged at equal angles about the nozzle circumference. The speakers were driven from a common oscillator through individual phase-shifting networks and power amplifiers. The phase-shifting networks permitted compensation for variations in phase between speakers and can be used to excite circumferential modes of instability. The gains of the amplifiers were individually adjusted to compensate for variations in speaker efficiency. Phase-locked averages were phase-locked to the oscillator signal.

3. Naturally occurring instabilities

Since the Crow & Champagne experiment the concept of a preferred mode has been generalized to include unexcited jets. In that case the preferred mode usually is defined as the passage frequency of the most energetic disturbance occurring near the end of the potential core. This frequency can be measured from a local peak in the power spectrum or from successive peaks in an autocorrelation function. In the case of the Crow & Champagne experiment the unexcited spectral peak occurred at $fD/U_j = 0.44$ (their figure 30). Gutmark & Ho (1983) have compiled spectral measurements by various investigators and the reported Strouhal numbers fD/U_j ranged from 0.24 to 0.51. Some of this scatter can be attributed to the inherent uncertainty in defining a unique timescale from a broadband signal. For example Petersen (1978) obtained spectral estimates from the same data base that varied by

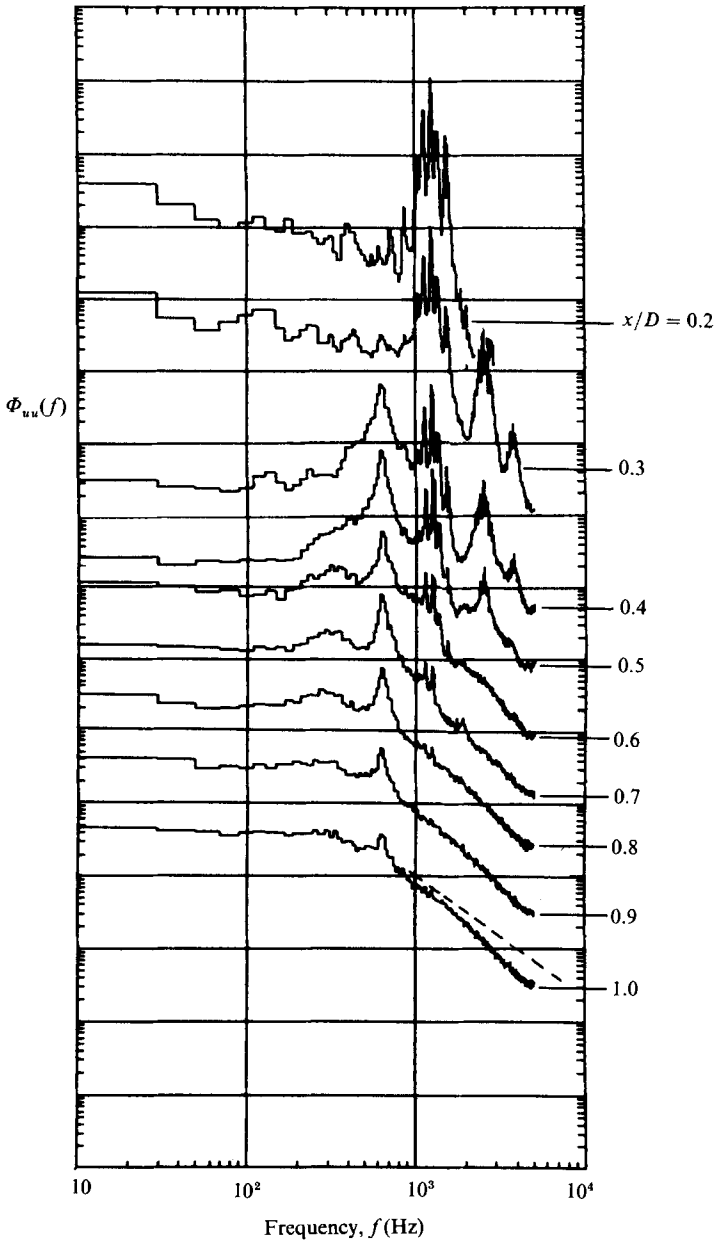

FIGURE 2. Power spectra of streamwise velocity measured at $r/D = 0.5$ and at various streamwise locations in the region of laminar to turbulent transition. ——, $-\frac{5}{3}$ spectral decay.

a factor of 2, depending on how the scale was defined. Even when a consistent spectral technique is used there is still some variation in the Strouhal number which can be related to boundary conditions at the nozzle exit. For example, Kibens (1981) and Drubka (1981) both observed a dependence of the Strouhal number on the initial momentum thickness. Ho & Hsiao (1983) observed essentially the same phenomenon in a planar jet.

The present jet shear layer was initially laminar as it issued from the nozzle. The transition to turbulent flow occurred within the first nozzle diameter downstream

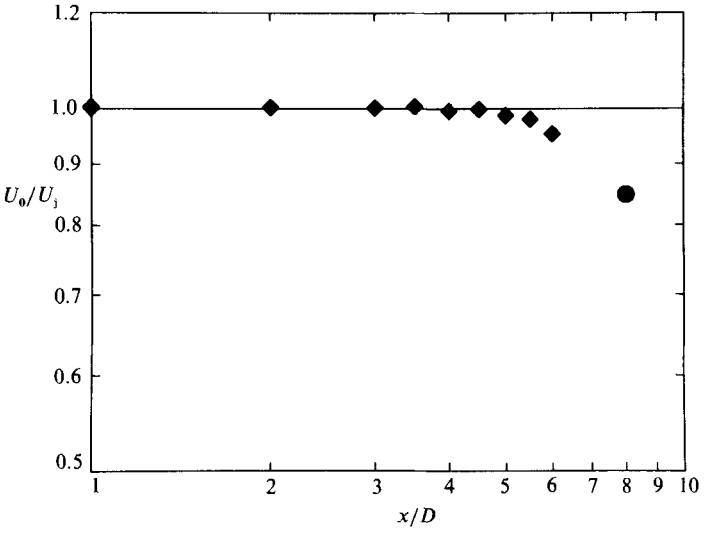

FIGURE 3. Distribution of centreline velocity.

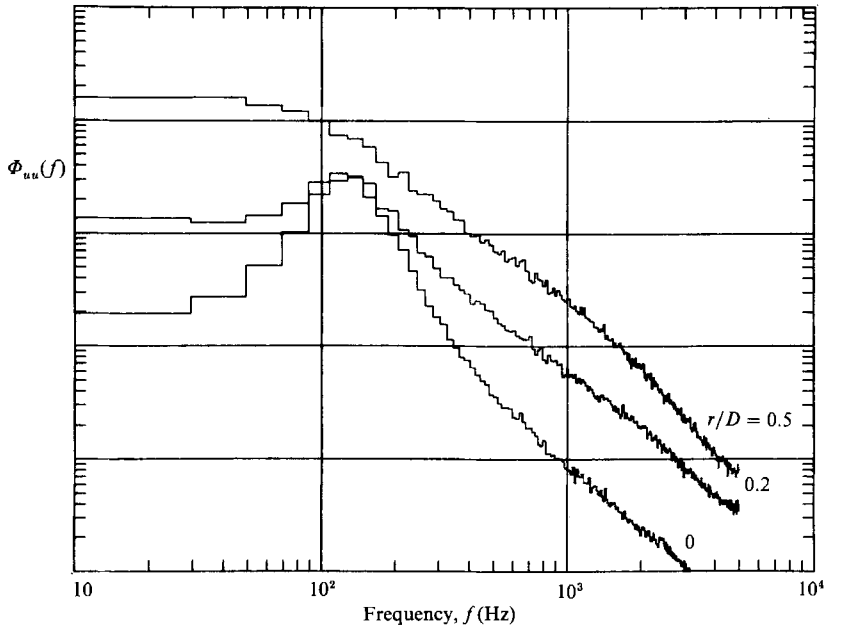

FIGURE 4. Power spectra of streamwise velocity measured at $x/D = 4.0$ and at various radial locations.

based on the emergence of the inertial subrange. Power spectra of the streamwise component of velocity, measured near the centre of the mixing layer ($r/D = 0.5$) at various streamwise locations, are shown in figure 2. Within the first diameter there were three local peaks in the spectra occurring at frequencies of roughly 1200, 600 and 300 Hz. The peak at 1200 Hz was produced by the local instability of the initial shear layer. The peaks at 600 Hz and 300 Hz evolved with streamwise distance and were produced by pairings or subharmonic resonances. By $x/D = 1.0$ the inertial subrange is evident from the $-\frac{5}{3}$ spectral decay.

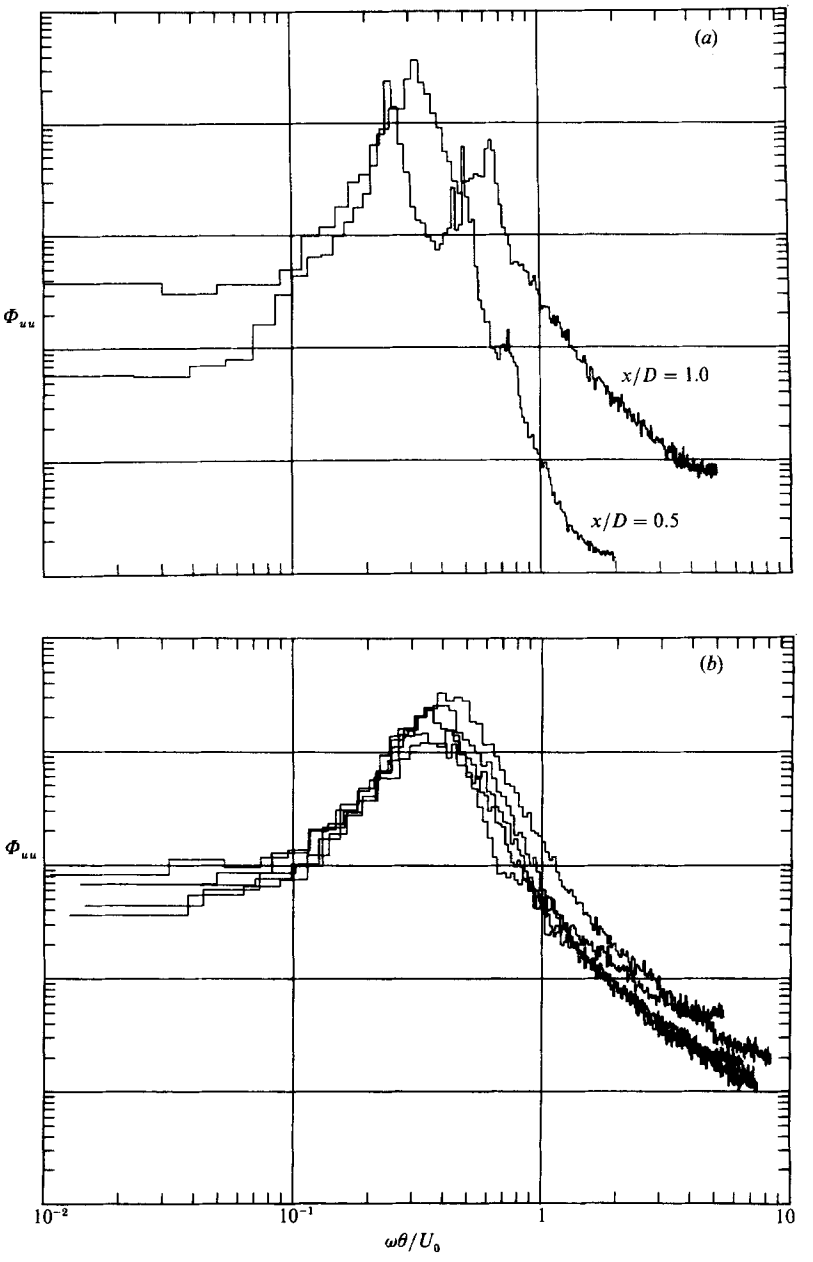

FIGURE 5. Power spectra of streamwise velocity measured along the inner edge of the mixing layer ($-7°$ ray) and scaled with local momentum thicknesses. (*a*) The region of laminar–turbulent transition; (*b*) the region extending from $x/D = 1.5$ to 4.0.

The end of the potential core is defined as the point where the developing mixing layers merge and completely fill the jet. Beyond that point the centreline velocity decays with streamwise distance. The measured distribution of centreline velocity, shown in figure 3, was obtained with a single hot-wire probe and was normalized by jet velocity U_j obtained from plenum pressure. Although the onset of centreline

velocity decay actually occurred at about 4.5 diameters from the jet exit the preferred mode is defined here as the natural instability observed at $x/D = 4.0$, in keeping with other investigators (e.g. Gutmark & Ho 1983).

The natural instability was determined from the velocity spectra shown in figure 4. At the centre of the mixing layer, $r/D = 0.5$, the spectrum is typical of fully developed turbulent flow and the large-scale coherent motion is obscured by fine-scale turbulence. However the passage of large-scale structures can be inferred from their near-field signatures induced by the coherent vorticity field (Mollo-Christensen 1967). The spectrum measured at the edge of the mixing layer, $r/D = 0$, exhibited a local peak at a frequency of 125 Hz. The corresponding Strouhal number based on jet diameter fD/U_j is 0.40 and is within the range of values compiled by Gutmark & Ho (1983). The three spectra are shown on the same absolute scale and it is apparent that the near field acts as a spatial filter that attenuates the broadband turbulence spectrum while leaving intact the spectral peak caused by the passage of the coherent structures.

The frequency of the natural instability is different at each streamwise location. The spatial evolution of the instability is shown in figure 5. Velocity power spectra were measured along the edge of the mixing layer at a polar angle of $-7°$ with respect to the nozzle lip. This is approximately the line extending from $(x/D, r/D) = (0, 0.5)$ to $(x/D, r/D) = (4.0, 0)$. In order to demonstrate that the natural instabilities scale with shear-layer thickness the frequencies are expressed as local Strouhal numbers $\omega\theta/U_0$, where U_0 is the local centreline velocity, ω is angular frequency ($2\pi f$), and θ is the local momentum thickness defined by

$$\theta = \int_0^\infty \frac{U(r)}{U_0}\left[1 - \frac{U(r)}{U_0}\right] \mathrm{d}r. \tag{3.1}$$

This is the usual frequency scaling used in stability analyses (e.g. Michalke 1971). Within the first diameter the spectral shift to subharmonic frequencies exhibited a rough scaling with local Strouhal number (figure 5*a*). Beyond $x/D = 1.5$ the power spectra collapsed to the same general curve with a peak near $\omega\theta/U_0 = 0.4$ (figure 5*b*). The stability calculations of Crighton & Gaster (1976), expressed in terms of local variables, predict $\omega\theta/U_0 = 0.34$ for the most amplified wave ($fD/U_0 = 0.38$ and $D/\theta = 7.1$). By combining the spectral data and momentum-thickness measurements of Drubka (1981, figures 37 and 70) the inferred $\omega\theta/U_0$ range from 0.32 to 0.39 at $x/D = 4.0$.

4. Viscous stability theory

The object of exciting the preferred mode artificially is to map the spatial evolution of the disturbance from phase-locked velocity measurements. Phase-locked measurements result in a periodic signal of *finite* amplitude superimposed on a quasi-parallel, mean velocity profile. Linear stability theory predicts the spatial structure and amplification of *infinitesimal* waves superimposed on a quasi-parallel, mean velocity profile. Some of the capabilities and limitations of linear theory to predict the evolution of coherent structures are now understood. For example linear theory is inadequate for predicting total amplification. Although there is a significant improvement when weak, non-parallel terms are retained, the predicted amplification is still much larger than the measured values (Wygnanski & Petersen 1987). That is

because the nonlinear exchange of energy from the disturbance to the mean flow or to other modes has been neglected. In order to correctly predict these interactions, second-order terms must be retained (Wygnanski, Marasli & Champagne 1987).

Non-parallel effects and weakly nonlinear effects are obtained by solving an amplitude equation. The eigenfunctions are obtained by solving a homogeneous equation that describes the stability of the locally parallel flow (e.g. Crighton & Gaster 1976; Plaschko 1979). The success of the perturbation theory then depends on the ability of the eigenfunctions, calculated from parallel stability theory, to describe transverse distributions of amplitude, phase, Reynolds stress, etc. Similarly, energy integral methods require shape assumptions that are based on eigenfunctions calculated from locally parallel, linear stability theory (e.g. Chan 1977; Tam & Morris 1985).

The stability equations can be formulated directly from the phase-locked equations of motion. Following Hussain & Reynolds (1970) the velocity field can be decomposed into the time-averaged velocity, a phase-locked disturbance, and a phase incoherent disturbance:

$$\boldsymbol{u} = \boldsymbol{U} + \hat{\boldsymbol{u}} + \boldsymbol{u}', \tag{4.1}$$

where the time average $\boldsymbol{U} = \bar{\boldsymbol{u}}$, the phase-locked disturbance $\hat{\boldsymbol{u}} = \langle \boldsymbol{u} \rangle - \boldsymbol{U}$, and the phase incoherent disturbance $\boldsymbol{u}' = \boldsymbol{u} - \langle \boldsymbol{u} \rangle$. The overbar denotes time average and the brackets denote phase-locked, ensemble average. Some time-averaged properties are

$$\overline{\hat{\boldsymbol{u}}} = 0; \quad \overline{\boldsymbol{u}'} = 0. \tag{4.2}$$

Some phase-locked, ensemble averages are

$$\langle \boldsymbol{u}' \rangle = 0; \quad \langle \hat{\boldsymbol{u}} \cdot \boldsymbol{u}' \rangle = 0 \tag{4.3}$$

and

$$\langle \boldsymbol{u} \cdot \boldsymbol{u} \rangle = \boldsymbol{U} \cdot \boldsymbol{U} + 2\hat{\boldsymbol{u}} \cdot \boldsymbol{U} + \hat{\boldsymbol{u}} \cdot \hat{\boldsymbol{u}} + \langle \boldsymbol{u}' \cdot \boldsymbol{u}' \rangle. \tag{4.4}$$

If the mean flow is assumed to be parallel, $\boldsymbol{U} = [U(r), 0, 0]$, then to first order the phase-locked equations of motion are

$$\nabla \cdot \hat{\boldsymbol{u}} = 0, \tag{4.5}$$

$$\frac{\partial \hat{\boldsymbol{u}}}{\partial t} + U\frac{\partial \hat{\boldsymbol{u}}}{\partial x} + \hat{v}\frac{\partial \boldsymbol{U}}{\partial r} = -\frac{1}{\rho}\nabla \hat{p} + \nu \nabla^2 \hat{\boldsymbol{u}}. \tag{4.6}$$

The viscous terms are retained in order to obtain damped eigensolutions when the disturbance has travelled beyond the point of neutral stability. Note that the molecular viscosity is appropriate to this formulation and that the mean velocity is a time average rather than a zone average. The assumption of small disturbance amplitude, which is implicit in this formulation, will be severely stretched in some of the measurements to follow.

The phase-locked velocity fluctuations are modelled by normal-mode perturbations of the form (Batchelor & Gill 1962; Lessen & Singh 1973; Morris 1976):

$$(\hat{u}, \hat{v}, \hat{w}, \hat{p}) = [F(r), \mathrm{i}G(r), H(r), P(r)]\, \mathrm{e}^{\mathrm{i}(\alpha x + m\phi - \omega t)} + \text{c.c.}, \tag{4.7}$$

where α is the complex wavenumber, ω is the angular frequency, and m is the spinning-mode number. The stability equations for an axisymmetric perturbation

are formulated by setting $m = 0$ and by substituting expressions (4.7) into the phase-locked equations of motion (4.5), (4.6). The resulting equations are

$$\alpha F + \frac{1}{r}\frac{\mathrm{d}}{\mathrm{d}r}(rG) = 0, \tag{4.8a}$$

$$\alpha(U-c)F + G\frac{\mathrm{d}U}{\mathrm{d}r} + \alpha P = -\frac{\mathrm{i}}{Re}\left[\frac{\mathrm{d}^2F}{\mathrm{d}r^2} + \frac{1}{r}\frac{\mathrm{d}F}{\mathrm{d}r} - \alpha^2 F\right], \tag{4.8b}$$

$$\alpha(U-c)G - \frac{\mathrm{d}P}{\mathrm{d}r} = -\frac{\mathrm{i}}{Re}\left[\frac{\mathrm{d}^2G}{\mathrm{d}r^2} + \frac{1}{r}\frac{\mathrm{d}G}{\mathrm{d}r} - \left(\alpha^2 + \frac{1}{r^2}\right)G\right], \tag{4.8c}$$

where c is the complex phase velocity ($c = \omega/\alpha$), and Re is the local Reynolds number ($Re = U_0\theta/\nu$). Equations (4.7)–(4.13) are written in non-dimensional form. The length and velocity scales are θ and U_0.

The boundary conditions on the perturbations are (Batchelor & Gill 1962)

$$F, G, P \to 0 \quad \text{as } r \to \infty, \tag{4.9a}$$

$$G = 0, \quad F, P \text{ finite at } r = 0. \tag{4.9b}$$

For a given velocity profile $U(r)$ and dimensionless frequency ω the radial profiles $F(r)$, $G(r)$, $P(r)$ are eigenfunctions and the complex wavenumber α is the eigenvalue.

In order to solve (4.8) numerically over a finite domain it is necessary first to obtain analytic solutions to the asymptotic equations for large and small r. If F and P are eliminated from (4.8) in favour of G the resulting fourth-order equation is similar to the Orr–Sommerfeld equation for two-dimensional flows:

$$\mathrm{D}^2\mathrm{D}^2G - \mathrm{i}\alpha\, Re\left[(U-c)\,\mathrm{D}^2G - rG\frac{\mathrm{d}}{\mathrm{d}r}\frac{1}{r}\frac{\mathrm{d}U}{\mathrm{d}r}\right] = 0, \tag{4.10}$$

where

$$\mathrm{D}^2 = \frac{\mathrm{d}^2}{\mathrm{d}r^2} + \frac{1}{r}\frac{\mathrm{d}}{\mathrm{d}r} - \left(\alpha^2 + \frac{1}{r^2}\right).$$

In the potential-core region of the jet, the mean velocity $U(r)$ approaches a constant value asymptotically at large and small values of r. Consequently derivatives of $U(r)$ vanish asymptotically. In those limits (4.10) assumes the following asymptotic forms:

$$[\mathrm{D}^2 - \mathrm{i}\alpha\, Re\,(1-c)]\,\mathrm{D}^2G = 0 \quad \text{at } r \to 0, \tag{4.11a}$$

$$[\mathrm{D}^2 + \mathrm{i}\alpha c\, Re]\,\mathrm{D}^2G = 0 \quad \text{at } r \to \infty. \tag{4.11b}$$

Equations (4.11) can be solved exactly in terms of modified Bessel functions:

$$G_0 = -A_1\frac{1}{\alpha}I_0'(\alpha r) - A_2\frac{\alpha}{Q^2}I_0'(Qr) \quad \text{at } r \to 0, \tag{4.12}$$

where

$$Q^2 = \alpha^2 + \mathrm{i}\alpha\, Re\,(1-c),$$

and

$$G_\infty = -A_3\frac{1}{\alpha}K_0'(\alpha r) - A_4\frac{\alpha}{Z^2}K_0'(Zr) \quad \text{at } r \to \infty, \tag{4.13}$$

where

$$Z^2 = \alpha^2 - \mathrm{i}\alpha c\, Re.$$

The first terms in (4.12) and (4.13) are independent of viscosity and resemble the inviscid solution for a cylindrical vortex sheet (Batchelor & Gill 1962). The other terms have been called the 'viscous correction mode'.

Equation (4.10) was written as four first-order differential equations which were integrated numerically using a standard fourth-order Runge–Kutta scheme. An iterative, shooting method was used to determine the eigenvalue. For the iterative procedure, the eigenvalue criterion of Lessen & Singh (1973) was used. At high Reynolds numbers ($Re > 500$) a normalization and orthogonalization technique (Bellman & Kalaba 1965) was employed to preserve the linear independence of the two solutions that form the eigenfunction.

In using the shooting method, the iteration procedure requires an initial estimate of the eigenvalue. The required accuracy of this estimate becomes critical at high Reynolds numbers where, owing to the orthonormalization procedure, the radius of convergence is quite small. In the present work, the approximate value of the eigenvalue was determined by employing a search scheme based on the 'argument principle' of Lessen, Sadler & Liu (1968). This technique has the added benefit that it can be used to determine whether the eigenvalue corresponds to the least stable radial mode for the particular values of Re and ω.

The stability calculations were based on measured velocity profiles. Gaster, Kit & Wygnanski (1985) showed that model profiles such as a hyperbolic tangent shape are inadequate if quantitative comparisons between measurement and theory are required. Since an analytic expression for $U(r)$ is required the measurements were fitted with profiles of the form

$$\left.\begin{aligned} \frac{U(r)}{U_0} &= 0.5[1-\tanh(\mu)]+C_1\,\mathrm{sech}^2(\mu)\tanh^2(\mu)+C_2\,\mathrm{sech}^4(\mu)\tanh(\mu), \\ \mu &= B(r/R_{0.5}-R_{0.5}/r), \end{aligned}\right\} \tag{4.14}$$

where $R_{0.5}$ is the half-velocity radius. The empirical constants C_1 and C_2 were determined from a least-squares fit to the data and provide symmetric and antisymmetric corrections to a basic tanh profile (Michalke 1971). These terms provide two independent degrees of freedom for matching general asymmetries. The constant B was adjusted so that the momentum thickness of the analytic profile matched the measured value.

Mean velocity profiles were measured without external excitation at streamwise positions ranging from $x/D = 0.25$ to $x/D = 5$. In each case the radial survey extended from $r/D = 0.19$ to the point where $U(r)/U_0 \leqslant 0.1$. Stability calculations were performed for each profile and the results were extrapolated to $x/D = 0$. For each profile the Strouhal number $\omega\theta/U_0$ was varied from 0 to 0.5 in increments of 0.01. The increments were reduced to 0.005 near the neutral point.

The imaginary and real parts of the eigenvalues resulting from the stability calculations are shown in figures 6 and 7 in the form of contour plots. The contour of neutral solutions is highlighted and the evolution of the preferred mode, 125 Hz, is indicated as a trajectory. The preferred mode was evidently a neutral wave by $x/D = 4.0$. The largest amplification rate $\alpha_i\theta = -0.125$ occurred near $x/D = 0.5$ and $\omega\theta/U_0 = 0.17$ (figure 6). It is interesting that the preferred-mode trajectory missed the peak by about an octave at $x/D = 0.5$. That may explain the observation by Crow & Champagne that the most efficient means of forcing the preferred mode was to excite the jet at the harmonic frequency $fD/U_0 = 0.6$.

There is a general decrease in amplification rates with increasing streamwise

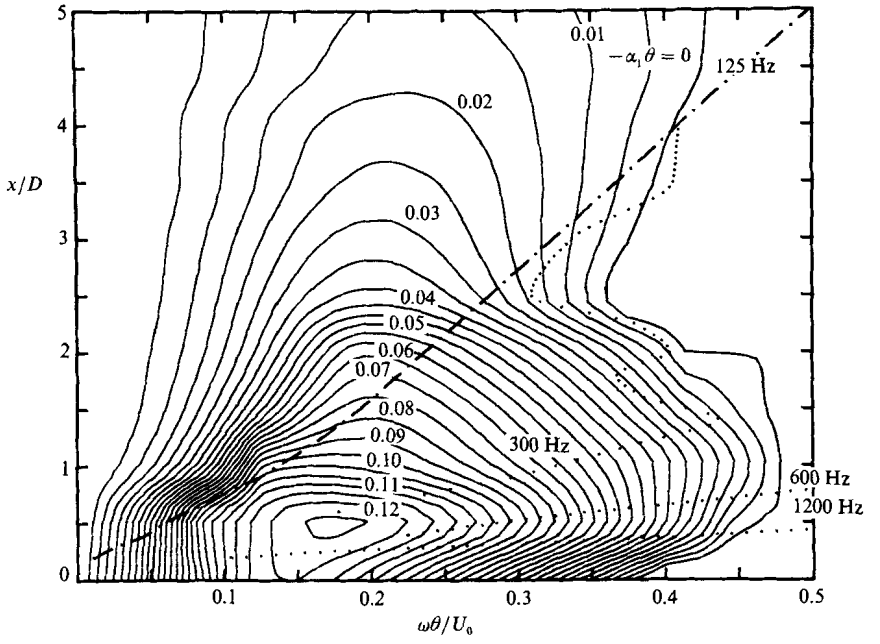

FIGURE 6. Contours of amplification rates computed from spatial stability theory: ·—·, 125 Hz excitation; ...., evolution of spectral peaks.

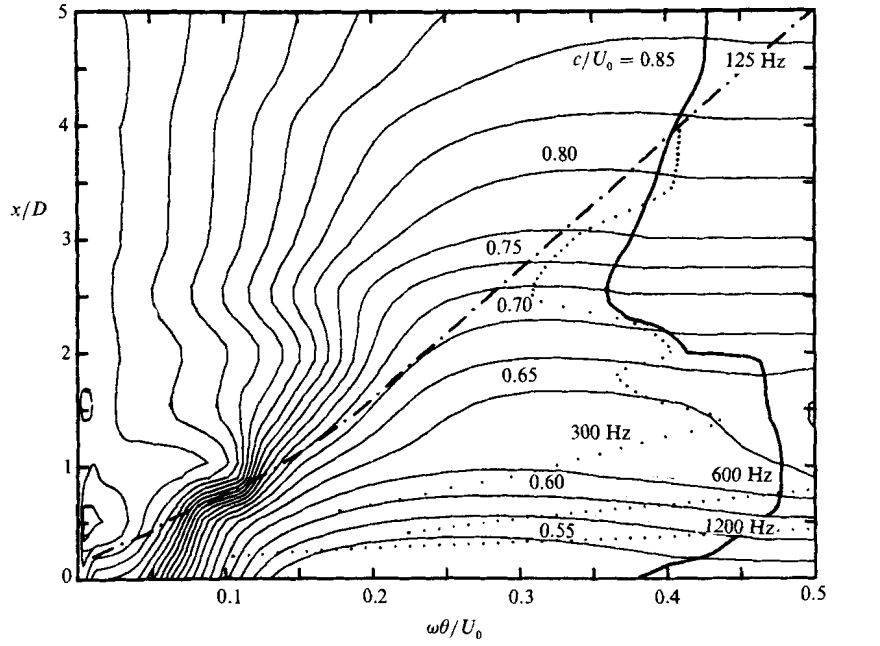

FIGURE 7. Contours of phase speeds computed from spatial stability theory.

distance x/D. At some point beyond the potential-core region there is a cutoff in axisymmetric instabilities. This has been predicted theoretically (Batchelor & Gill 1962; Morris 1976) and observed experimentally (Dimotakis, Lye & Papantoniou 1983) in the far jet. This cutoff phenomenon may account for the impression based on flow visualization that the near-jet region is dominated by a single axisymmetric

lengthscale. That lengthscale in fact corresponds to the most amplified instability, as predicted by Crighton & Gaster (1976).

Variations in spectral-peak Strouhal number can also be explained based on the eigenvalue contours. Trajectories of peak Strouhal numbers from figure 5 are superimposed on the amplification rate contours in figure 6. The frequency of the initial instability was 1200 Hz. Subharmonic peaks at frequencies of 600 Hz and 300 Hz emerged farther downstream at locations where the associated fundamental was approaching the neutral point. This frequency selection is related to the dispersion relationship. Contours of dimensionless phase velocity $c/U_0 = \omega/\alpha_r U_0$, figure 7, show that high-Strouhal-number disturbances are relatively non-dispersive. A subharmonic resonance between amplified disturbances requires a range of non-dispersive frequencies that extends at least an octave below the neutral frequency (Petersen 1978). The frequency range of non-dispersive waves, figure 7, decreased with downstream distance, and beyond $x/D = 2.0$ the range was less than an octave. The subharmonics occurred within the first two diameters and beyond that point there was a continuous shift in frequency until $x/D = 4.0$ where the spectral peak and the 125 Hz trajectory coincided. The frequency of the spectral peak in this region generally tracked the contour of neutral growth rate. This behaviour is consistent with the usual observation (e.g. Schubauer & Skramstad 1947) that the maximum total amplification at fixed frequency occurs at the location of the neutral point.

5. Preferred mode with external excitation

It is necessary to document the boundary conditions in free-jet measurements if one wishes to make detailed predictions of spectral trends. This was demonstrated by the measurements of Cohen & Wygnanski (1987) taken in the initial, laminar region of a jet. The most energetic disturbance was not necessarily the most amplified disturbance but it could be predicted accurately by applying linear stability theory as a two-point transfer function to the 'background' turbulence spectrum measured near the exit plane. Alternatively, the boundary conditions can be controlled through external excitation. Not only are the boundary conditions determined but the unsteady flow field can be mapped by means of phase-locked averages.

External excitation was used in order to map the spatial structure of the preferred mode by means of phase-locked velocity. The frequency of the excitation was 125 Hz and was based on the frequency of the unforced spectral peak, figure 4. Two excitation levels were used in the present study and they will be identified by the parameter $e = 1$ or 4, proportional to the level. The low level was selected to 'tag' the preferred mode without changing the flow while the high level was selected to produce significant finite-amplitude effects.

An important feature of the original Crow & Champagne experiment was the global sensitivity of the flow to the level of excitation. When the excitation was strong not only did the excited disturbance saturate but the flow itself was fundamentally altered. The jet spreading rate was increased and the broadband turbulence spectrum was changed. Active control of the flow by high level excitation has important technological implications and one would like to know how the structure of the instability is affected. One would also like to relate the excited disturbance to instabilities occurring naturally in the flow. Part of the difficulty comes from the different types of signal processing techniques used to educe coherent structures in excited *vs.* unexcited flows. A phase-locked average is a filter that in principle can be applied to the total data record whereas a conditional sample is a

zone average that is limited usually to a minute fraction of the record. It is an open question which average is more representative of the natural flow. However, Hussain & Zaman (1981) did note a qualitative similarity between their phase-locked data taken in an excited jet and the conditionally sampled measurements of Yule (1978).

The point of view adopted here is that coherent structures are instabilities that result mainly from the linear and nonlinear evolution of disturbances present at the boundary where the flow separates from the nozzle. That has been shown to be the case at the point of laminar to turbulent transition (Cohen & Wygnanski 1987). In order to tag a 'natural' coherent structure it is sufficient to ensure that the natural disturbances present at the nozzle exit are not dominated by the artificial disturbance. The phase-locked average then recovers only that fraction of the evolved disturbances that remains temporally coherent with the excitation.

The effect of excitation level on the turbulence power spectrum is presented in figure 8, which was measured on the jet centreline at $x/D = 4.0$. At the lower excitation level the disturbance was simply superimposed on the natural spectrum. At the higher excitation level there was considerable nonlinear distortion of the entire spectrum. Turbulence levels were increased at frequencies below the excitation and suppressed at frequencies within an octave above the excitation.

Some of the spectral distortion at the higher level of excitation can be attributed to changes in the mean flow. Momentum thicknesses were calculated from the analytic profiles, (4.8), fitted to the measured velocity profiles and the spatial evolution is shown in figure 9. At the high excitation level the growth of the momentum thickness was accelerated owing to the increased entrainment rate whereas at the low excitation level the changes in the base flow were insignificant over the first four diameters.

Distortion of the mean flow altered the stability of the flow because the stability eigenmodes depend on both the shape and the thickness of the shear layer. The spatial distributions of calculated growth rate of the preferred mode, $f = 125$ Hz, are shown in figure 10 based on measured velocity profiles at both levels of excitation. By $x/D = 4.0$ the slightly excited shear layer remained unstable ($\alpha_i \theta = -0.008$) whereas the higher excitation resulted in a stable profile ($\alpha_i \theta = 0.036$).

The phase reference of the phase-locked velocity fluctuations $\langle u(r, \phi, \tau) \rangle$ was based on the signal from the oscillator used to drive the speaker array. The time τ is defined as the time increment from the phase reference. At each streamwise location phase-locked velocity histories were measured over a range of radial locations. Amplitude profiles were obtained by calculating Fourier coefficients:

$$F_{mn}(r) = \frac{1}{2\pi T} \int_0^{2\pi} \int_0^T \langle u(r, \phi, \tau) \rangle \exp\left\{ \mathrm{i} \left[m\phi - \frac{2\pi n \tau}{T} \right] \right\} \mathrm{d}\tau \, \mathrm{d}\phi. \tag{5.1}$$

Typical phase-locked velocity histories are shown in figure 11. Each value of $\langle u(r, \phi, \tau) \rangle$ is an ensemble average of 200 individual events, and the measurements have been Fourier transformed over circumferential angle ϕ. In this case the jet was excited at the high level. When the histories are transformed over delay time τ each radial position yields a single value of the Fourier coefficient $F_{mn}(r)$. Note that the maximum amplitude is about $0.1 U_0$ and that the velocity fluctuations are out of phase across the mixing layer.

The preferred mode is compared to stability theory in figure 12. Radial profiles of the Fourier coefficient $F_{01}(r)$, corresponding to the axisymmetric ($m = 0$) mode and

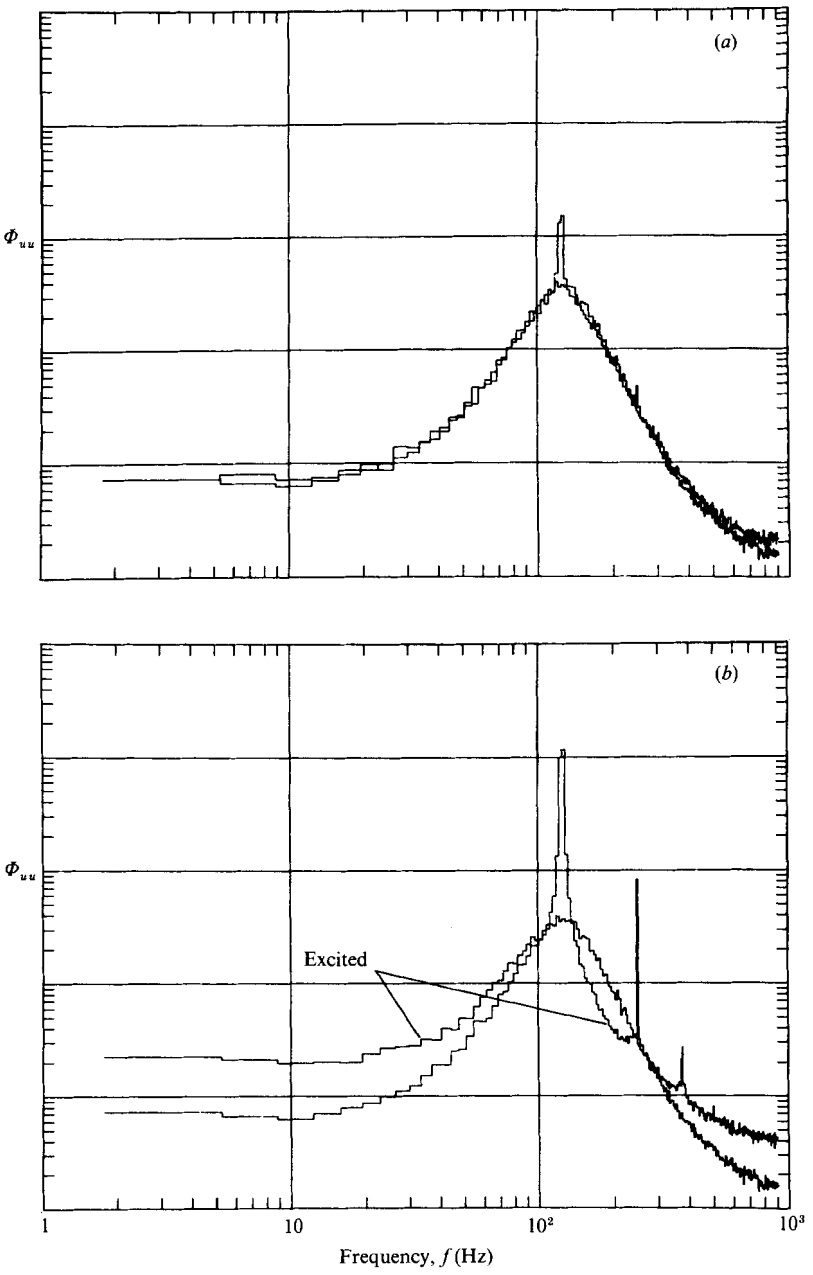

FIGURE 8. Effects of 125 Hz excitation on power spectra of streamwise velocity at $(x/D, r/D) = (4.0, 0)$. Unexcited spectra are superimposed for comparison. Excitation level: (*a*) $e = 1$; (*b*) $e = 4$.

the fundamental ($n = 1$) excitation frequency, are superimposed on the corresponding eigenfunctions. Stability eigenfunctions can be determined only to within a constant. In order to compare profiles shapes the eigenfunction magnitudes were normalized to match the area under the measured profile, and the phase angles were set to zero on the high-velocity side. The radial coordinate is expressed in terms of the similarity parameter η defined by

$$\eta = (r - R_{0.5})/\theta. \tag{5.2}$$

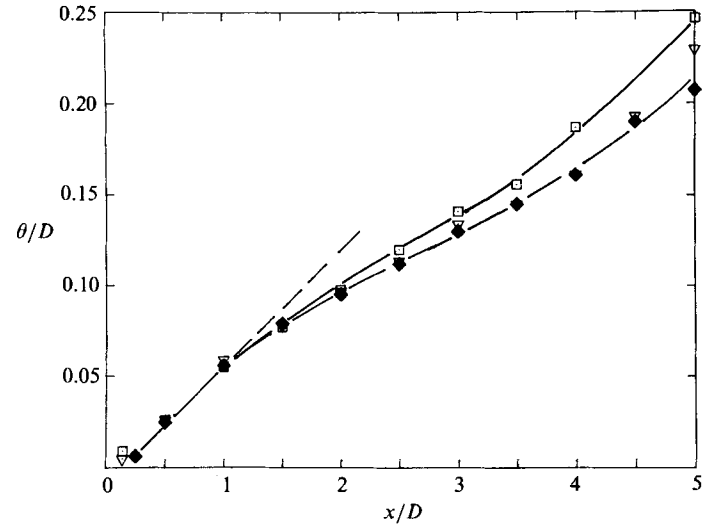

FIGURE 9. Effect of excitation level on the growth of the momentum thickness. Excitation level at 125 Hz: ◆ $e = 0$; ▽ $e = 1$; ⊡ $e = 4$.

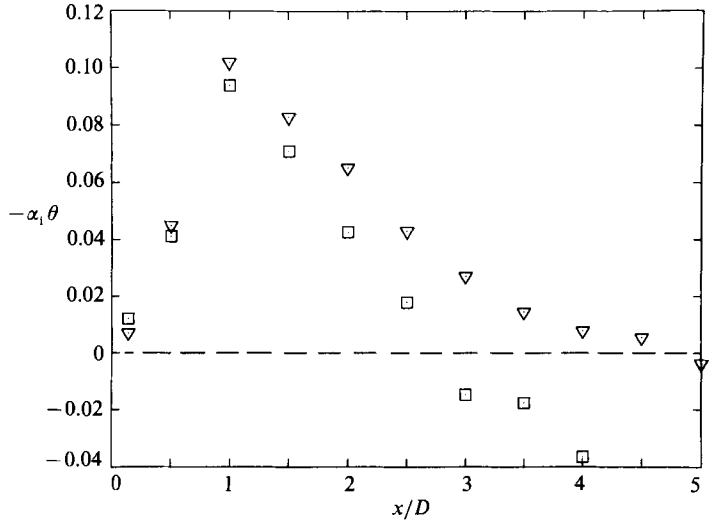

FIGURE 10. Effect of excitation level on the computed, local stability of the preferred mode. Stability calculations are based on local, measured velocity profiles. Symbols same as in figure 9.

The general agreement between measurement and theory is good and the radial locations of maxima and minima are correctly predicted. There is no apparent deterioration in the agreement at the high excitation level even though the amplitude was nearly 10% of the jet velocity and even though the stability mode was locally damped.

The spatial evolution of the preferred mode at the low excitation level is shown in figures 13 and 14. The stability eigenfunctions are shown as solid lines. There were significant changes in the shapes of the profiles and the agreement between measurement and calculation is quite good. It is apparent that the preferred mode evolves as a local, shear-layer instability. Similar quantitative agreement was

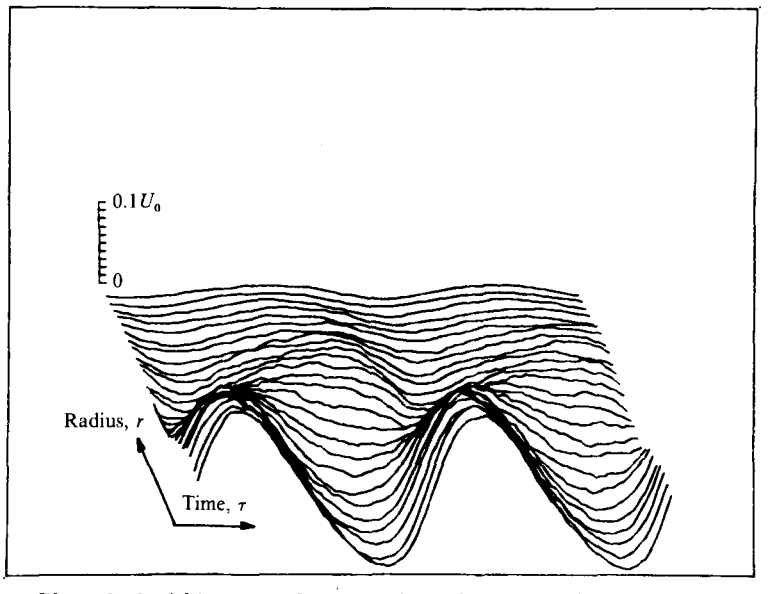

FIGURE 11. Phase-locked histories of streamwise velocity at $x/D = 4.0$. The histories are averages over the eight-wire array. Excitation: 125 Hz, $e = 4$.

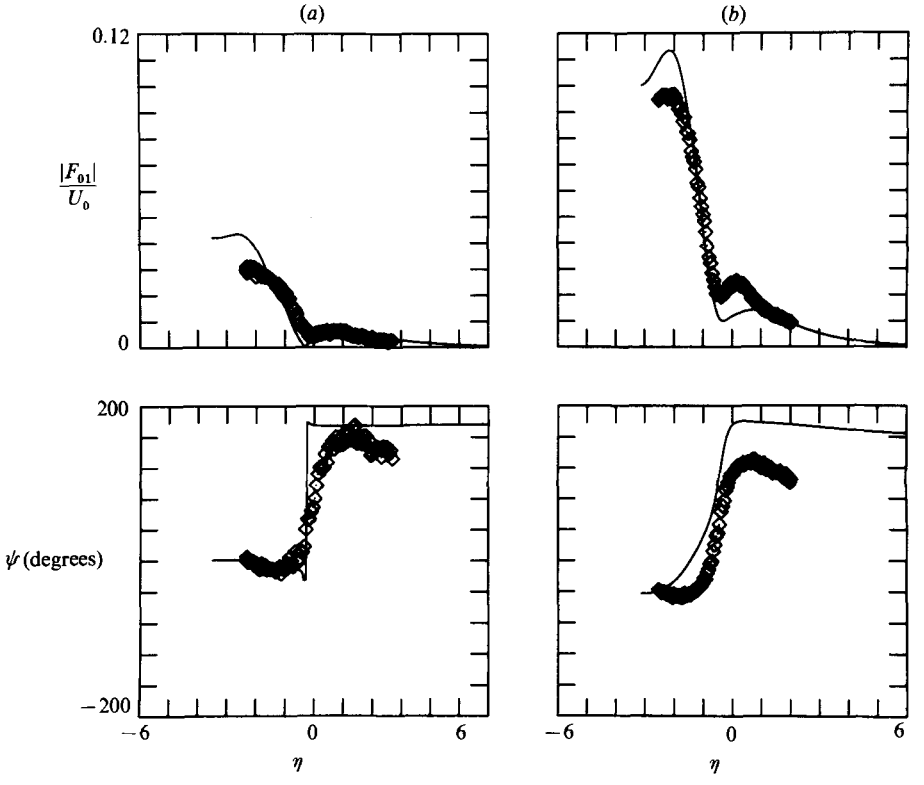

FIGURE 12. Radial profiles of phase-locked amplitudes and phase delays compared to stability eigenfunctions at $x/D = 4.0$. Excitation level at 125 Hz: (*a*) $e = 1$; (*b*) $e = 4$.

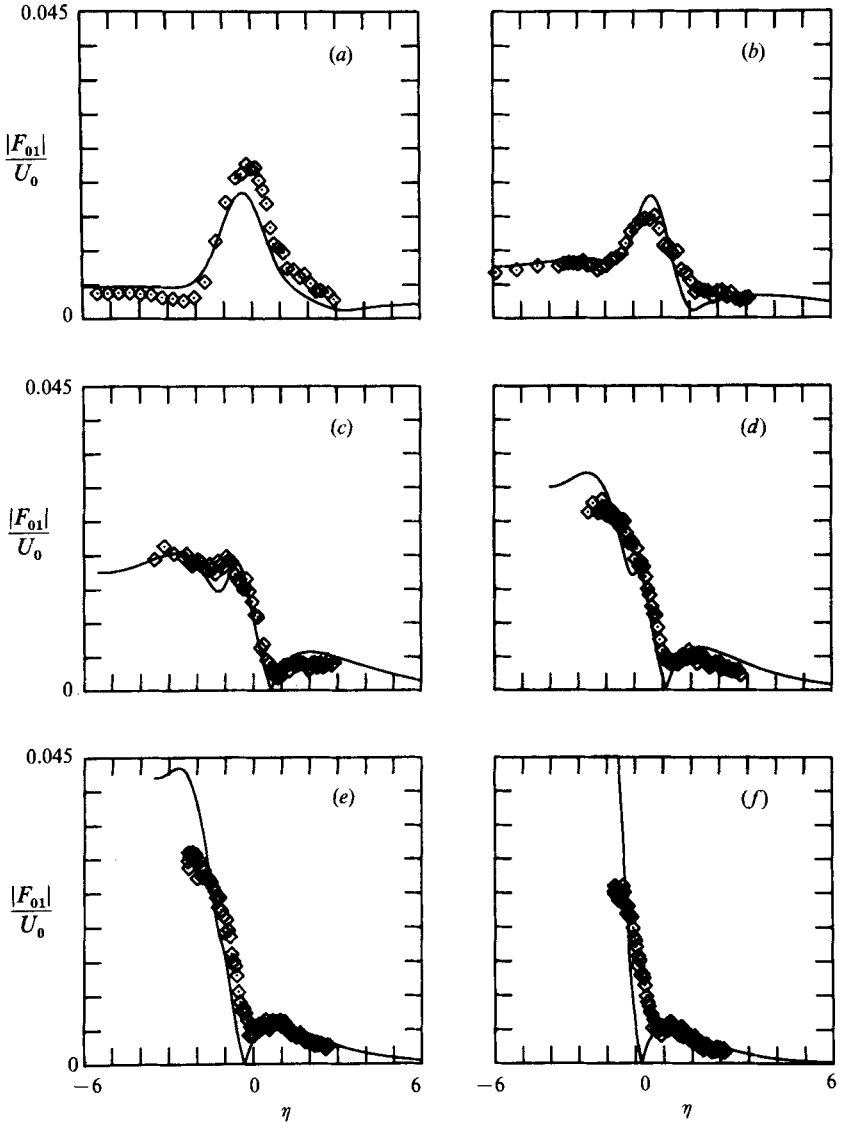

FIGURE 13. Spatial evolution of phase-locked amplitude profiles compared to stability eigenfunctions. Excitation: 125 Hz, $e = 1$. Measurement location x/D: (*a*) 0.5; (*b*) 1.0; (*c*) 2.0; (*d*) 3.0; (*e*) 4.0; (*f*) 5.0.

attained at the high excitation level. The decrease in the range of η towards the end of the potential core was caused by the travel of the radial traversing mechanism being fixed whereas the momentum thickness increased.

The calculated phase speeds are compared to measurements in figure 15. Since the flow is dispersive it is the advance in phase angle that is actually measurable. The phase advance along rays of constant η can be calculated from α_r, the real part of the streamwise wavenumber, according to

$$\psi(x, \eta) = \psi(x_0, \eta) + \int_{x_0}^{x} \alpha_r(x, \eta)\, \mathrm{d}x. \tag{5.3}$$

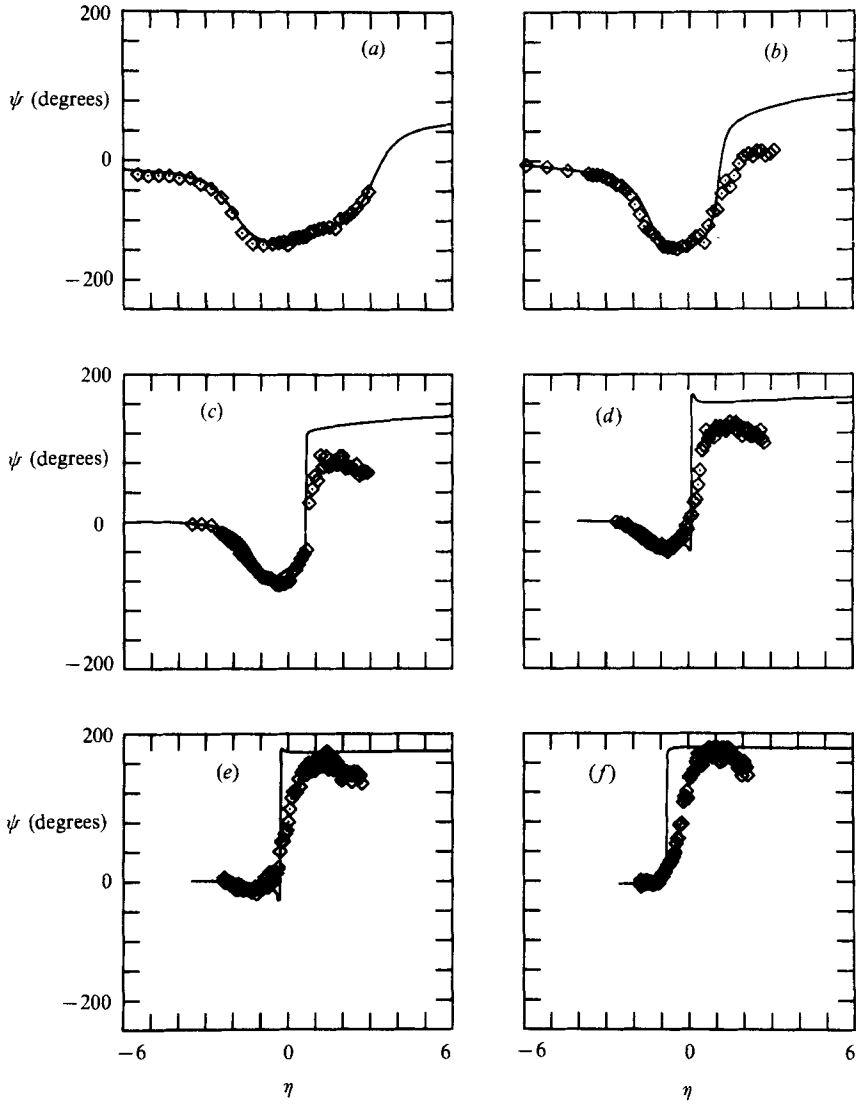

FIGURE 14. Spatial evolution of phase delay profiles compared to stability eigenfunctions. Same conditions as in figure 13.

The measurements were made along the high-speed side ($r/D = 0.2$) of the jet mixing layer and the agreement with parallel, stability theory is excellent. The phase speed measured by Crow & Champagne at $(x/D, r/D) = (4.0, 0)$ are included to show that the present measurements are consistent with theirs. It must be noted that phase speeds calculated on the basis of a parallel mean flow are uniform across the flow whereas the measured phase advance varies across the flow. This effect can be taken into account within the linearized theory by retaining weak non-parallel terms (Crighton & Gaster 1976). For that reason the present calculations should be regarded as an approximation. The approximation may be reasonably good because the phase angles change slowly with radius on the high-speed side and because the measurements were made near the critical layer.

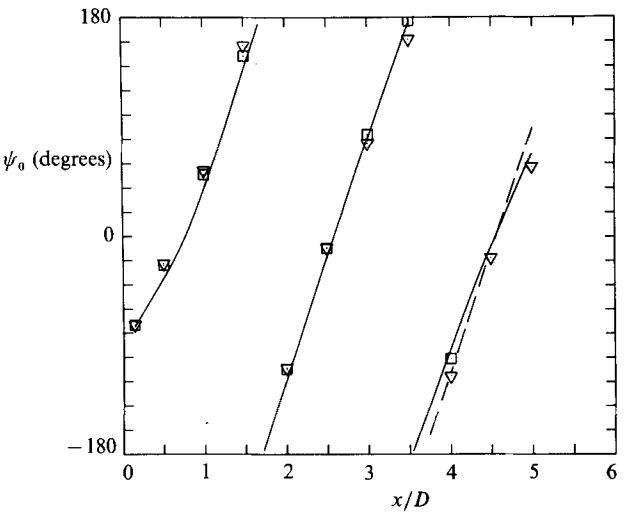

FIGURE 15. Phase advance measured at $r/D = 0.2$ compared to stability computations: —, stability theory; – –, Crow & Champagne (1971).

6. Discussion

The streamwise distribution of natural instabilities were measured in the axisymmetric mixing layer of a low-speed air jet of moderate Reynolds number. The preferred mode was excited artificially and its spatial evolution was mapped using phase-locked velocity measurements. Based on those sets of measurements we can make the following observations.

(i) Within the first four diameters downstream of the nozzle exit plane the natural instabilities scaled with local shear-layer thickness rather than jet diameter. The distribution of passage frequencies associated with the instabilities could be explained from spatial stability theory provided the calculations were based on measured profiles of mean velocity.

(ii) The spatial structure of the preferred mode agreed with eigenfunctions calculated from the Orr–Sommerfeld stability equations based on measured velocity profiles. There was no apparent deterioration in the agreement between measurement and theory at high excitation levels even though there was considerable mean flow distortion and even though phase-locked amplitudes reached levels near 10% of the jet speed. There was no apparent deterioration between measurement and theory even at streamwise locations where the stability eigenmodes were locally damped.

(iii) By implication, there is no single preferred mode. The Orr–Sommerfeld eigenmodes scale with local shear-layer thickness. Jet diameter enters only as a parameter. The most amplified shear-layer mode depends on streamwise location and on the streamwise distribution of local shear-layer thickness.

Nevertheless flow-visualization experiments seem to suggest that the near-jet region is dominated by a single, axisymmetric lengthscale. It is our view that this impression is the result of a cutoff in the axisymmetric mode that occurs near the end of the potential core, rather than an indication of a global instability. Spatial stability theory predicts that helical instabilities become dominant beyond $x/D = 4$ (Michalke & Hermann 1982) and in the fully developed region axisymmetric disturbances are damped (Batchelor & Gill 1962; Morris 1976). In fact, flow visualization of the far jet suggests that the preferred mode is helical and has a

lengthscale commensurate with the local shear-layer thickness (Dimotakis *et al.* 1983).

The authors would like to thank Professors I. Wygnanski and F. Champagne for their comments and technical advice. The work was supported in part by the National Science Foundation under grant MEA 8210876 and by NASA-Lewis Research Center under grant NAG 3-460.

REFERENCES

Batchelor, G. K. & Gill, A. E. 1962 Analysis of the stability of axisymmetric jets. *J. Fluid Mech.* **14**, 529–551.

Bellman, R. E. & Kalaba, R. E. 1965 *Quasi-linearization and Non-linear Boundary-value Problems*. Elsevier.

Chan, Y. Y. 1977 Wavelike eddies in a turbulent jet. *AIAA J.* **15**, 992–1001.

Cohen, J. & Wygnanski, I. 1987 The evolution of instabilities in the axisymmetric jet. *J. Fluid Mech.* **176**, 191–235.

Crighton, D. G. & Gaster, M. 1976 Stability of slowly diverging jet flow. *J. Fluid Mech.* **77**, 397–413.

Crow, S. C. & Champagne, F. H. 1971 Orderly structure in jet turbulence. *J. Fluid Mech.* **48**, 547–591.

Dimotakis, P. E., Lye, R. C. & Papantoniou, D. Z. 1983 Structure and dynamics of round turbulent jets. *Phys. Fluids* **26**, 3185–3192.

Drubka, R. E. 1981 Instabilities in the near field of turbulent jets and their dependence on initial conditions and Reynolds number. Ph.D. Dissertation, Illinois Institute of Technology, Chicago.

Gaster, M., Kit, E. & Wygnanski, I. 1985 Large-scale structures in a forced turbulent mixing layer. *J. Fluid Mech.* **150**, 23–39.

Gutmark, E. & Ho, C. M. 1983 On the preferred modes and the spreading rates of jets. *Phys. Fluids* **26**, 2932–2938.

Ho, C. M. & Hsiao, F. B. 1983 Evolution of coherent structures in a lip jet. In *Structure of Complex Turbulent Shear Layers* (ed. R. Dumas & L. Fulachier), pp. 121–136. Springer.

Hussain, A. K. M. F. & Reynolds, W. C. 1970 The mechanics of an organized wave in turbulent shear flow. *J. Fluid Mech.* **41**, 241–258.

Hussain, A. K. M. F. & Zaman, K. B. M. Q. 1981 The 'preferred mode' of the axisymmetric jet. *J. Fluid Mech.* **110**, 39–71.

Kibens, V. 1981 The limit of initial shear layer influence on jet development *AIAA Paper 81-1960*.

Lessen, M., Sadler, S. G. & Liu, T. Y. 1968 Stability of pipe Poiseuille flow. *Phys. Fluids* **11**, 1404–1408.

Lessen, M. & Singh, P. J. 1973 The stability of axisymmetric free shear layers. *J. Fluid Mech.* **60**, 433–457.

Michalke, A. 1971 Instabilität eines Kompressiblen runden Freistrahls unter Berücksichtigung des Einflusses der Strahlgrenzschichtdicke. *Z. Flugwiss.* **19**, 319–328.

Michalke, A. & Hermann, G. 1982 On the inviscid instability of a circular jet with external flow. *J. Fluid Mech.* **114**, 343–359.

Mollo-Christensen, E. 1967 Jet noise and shear flow instability seen from an experimenter's viewpoint. *Trans. ASME* E: *J. Appl. Mech.* **34**, 1–7.

Morris, P. J. 1976 The spatial viscous instability of axisymmetric jets. *J. Fluid Mech.* **77**, 511–529.

Petersen, R. A. 1978 Influence of wave dispersion on vortex pairing in a jet. *J. Fluid Mech.* **89**, 469–495.

Plashko, P. 1979 Helical instabilities of slowly divergent jets. *J. Fluid Mech.* **92**, 209–215.

SCHUBAUER, G. B. & SKRAMSTAD, H. K. 1947 Laminar boundary-layer oscillations and transition on a flat plate. *J. Aero. Sci.* **14**, 69–78.

TAM, C. K. W. & MORRIS, P. J. 1985 Tone excited jets, part V: a theoretical model and comparison with experiment. *J. Sound Vib.* **102**, 119–151.

WYGNANSKI, I., MARASLI, B. & CHAMPAGNE, F. H. 1987 On the weakly nonlinear stability model applied to a diverging small-deficit wake. *AIAA Paper 87-1465.*

WYGNANSKI, I. & PETERSEN, R. A. 1987 Coherent motion in excited free shear flows. *AIAA J.* **25**, 201–213.

YULE, A. J. 1978 Large-scale structure in the mixing layer of a round jet. *J. Fluid Mech.* **89**, 413–432.